

# On how neural networks enhance quantum state tomography with constrained measurements

Hailan Ma<sup>1</sup>, Daoyi Dong<sup>1,2</sup>, Ian R. Petersen<sup>2</sup>, Chang-Jiang Huang<sup>3</sup>, Guo-Yong Xiang<sup>3</sup>

<sup>1</sup> School of Engineering and Technology, University of New South Wales, Canberra, ACT 2600, Australia

<sup>2</sup> CIICADA Lab, School of Engineering, The Australian National University, Canberra, ACT 2601, Australia

<sup>3</sup> Key Laboratory of Quantum Information, University of Science and Technology of China, Chinese Academy of Sciences, Hefei 230026, China

E-mail: daoyi.dong@anu.edu.au

**Keywords:** Quantum state tomography, neural networks, quantum optical states, experimental noise

**Abstract.** Quantum state tomography aiming at reconstructing the density matrix of a quantum state plays an important role in various emerging quantum technologies. Inspired by the intuition that machine learning has favorable robustness and generalization, we propose a deep neural networks based quantum state tomography (DNN-QST) approach, which are applied to three measurement-constrained cases, including few measurement copies and incomplete measurements as well as noisy measurements. Numerical results demonstrate that DNN-QST exhibits a great potential to achieve high fidelity for quantum state tomography with limited measurement resources and can achieve improved estimation when tomographic measurements suffer from noise. In addition, the results for 2-qubit states from quantum optical devices demonstrate the generalization of DNN-QST and its robustness against possible error in the experimental devices.

## 1. Introduction

Quantum state tomography (QST), which aims at reconstructing the state of a quantum system via quantum measurements [1, 2] has drawn considerable efforts, owing to its significant role in verifying and benchmarking quantum tasks, including quantum computation [3], quantum control [4] and quantum communication [5]. To estimate a quantum state, a large number of measurements on an ensemble of identical quantum systems are performed to deduce its density matrix based on the measured outcomes. Several effective methods for QST have been proposed. Among them, least-squares inversion aims at solving the inverse of linear equations that relate the measured quantities to the density-matrix elements of a quantum system [6]. Bayesian tomography constructs a state using an integral averaging over all possible quantum states with proper weights [7, 8]. Maximum likelihood estimation (MLE) chooses the state estimate that maximizes the probability of the observed data, whose solution usually involves a large number of nonlinear equations [9, 10]. Linear regression estimation (LRE) solves the quantum state estimation problem using a linear model, and is usually combined with physical projection techniques to avoid the non-physical quantum states [11, 12].

Owing to its intrinsic capability of exacting information from high-dimensional data [13, 14], machine learning (ML) has been recently utilized to address various quantum tasks [15]. Among them, the representation of many-body quantum states [16], the verification of quantum devices [17], quantum error correction [18], quantum manipulation [19, 20] and quantum data compression [21, 22] have been investigated. QST is a process of extracting useful information from experimental measurement statistics [10] and can be naturally regarded as a data processing problem. Recently, there have been many efforts to investigate the use of ML in QST. For example, deep learning based QST has been proposed to reconstruct states [23, 24]. A convolutional neural network has been introduced to reconstruct 2-qubit quantum states from a set of coincidence measurements [25, 26, 27]. Reconstruction of optical quantum states with reduced data can be achieved via the utilization of conditional generative adversarial networks [28, 29]. ML has also been used to enhance the performance of experimental quantum state estimation [27, 30]. For example, neural networks act as a useful tool to denoise the state-preparation-and-measurement errors [31] and have achieved improved performance when combined with MLE. In [30], QST using neural networks has been benchmarked and compared on experimentally generated 2-qubit entangled states.

As is known, at least  $(4^n - 1)$  real parameters are required to specify the density matrix of an  $n$ -qubit quantum state, which means that the required measurement resources scale exponentially with the qubit number  $n$  [32]. For solid-state systems, the measurement process can be time-consuming, which can limit the time available for performing measurements during the data collection procedure. Under limited measurement copies, the approximation of the observed distributions for systems with large sizes tends to be undersampled, resulting in inaccurate measured statistics. From this perspective, the number of copies plays an essential role for practical QST. Hence, it

is meaningful to investigate the case of few measurement copies, which provides insight for QST on large quantum systems.

To determine a unique state, an informationally complete set of measurement operators is required. For example, 2-qubit state tomography relies on the measured statistics of at least 16 measurements [33]. In many solid-state systems, correlated multi-qubit measurement may not be realizable and experimental readout is often done via single-qubit projective operator measurements or single-spin measurements [34, 35]. In such cases, the measurement operators may be incomplete. Although incomplete measurements do not characterize a unique state, additional constraints can be introduced to obtain physically valid estimates [36]. For example, the maximum entropy principle finds a state consistent with the measured data with the largest von Neumann entropy [37, 38]. Variational quantum tomography returns a physically valid state that minimizes the expectation values of the missing operators [39]. Hence, we also investigate the performance of machine learning aided QST in the case of incomplete measurements.

In real applications, quantum measurements are prone to errors and noise, which increases the difficulty of characterizing quantum states with high efficiency. For example, it has been found that the computational resources to fully characterize a quantum state scale as  $O(d^4)$  when the observed data suffers from Gaussian noise [40]. Owing to the favorable generalization properties of neural networks [26, 14], we incorporate neural networks into QST to reconstruct quantum states using noisy measurements.

Considering that neural networks have the potential to characterize the features of quantum states [41, 42, 43] and usually require reduced prior knowledge about quantum states [41], we propose a deep neural networks based quantum state tomography (DNN-QST) approach, that can be applied in cases of few measurement copies and incomplete measurements. To demonstrate its capability and efficiency, simulations are performed on different cases for comparison with traditional methods. A significant improvement of average fidelity over MLE and LRE demonstrates the advantage of DNN-QST in reconstructing quantum states with limited measurement resources. In addition, DNN-QST is applied to noisy measurements and exhibits favorable robustness in reconstructing quantum optical states when tomographic measurements suffer from noise.

The rest of this paper is organized as follows. In Section 2, the DNN-QST method is presented in detail. Numerical results of QST with limited resources, i.e., few measurement copies and incomplete measurements are provided in Section 3. Section 4 investigates the performance of QST with noise. Concluding remarks are given in Section 5.

## 2. Deep neural networks based quantum state tomography

In this section, a machine learning aided quantum state tomography method (called as DNN-QST) that takes advantage of deep neural networks to reconstruct quantum states is proposed. Quantum state generation and its representation are firstly presented, and then quantum measurement settings are introduced. Finally, the DNN-QST method is provided in detail.

### 2.1. Quantum state generation and its representation

In this work, we first consider pure states. Let  $\mathbb{U}^d$  be the set of all  $d$ -dimensional unitary operators, i.e., any  $U \in \mathbb{U}^d$  satisfies  $UU^\dagger = U^\dagger U = \mathbb{I}_d$ . Owing to its invariance under group multiplication (i.e., any region of  $\mathbb{U}^d$  carries the same weight in a group average) [44], the Haar metric is utilized as a probability measure on a compact group. As such, random pure states can be generated by performing random unitary transformations following the Haar measure [12, 26], which can be formulated as  $|\psi\rangle_{haar} = U_{haar}|\psi_0\rangle$ , where  $|\psi_0\rangle$  is a fixed pure state.

In addition, we also consider mixed states in the following form

$$\rho_p = p|\psi\rangle\langle\psi|_{haar} + (1-p)\frac{\mathbb{I}_d}{d}, \quad (1)$$

where  $p \in (0, 1)$  represents the ratio of pure element. The purity of the quantum state in Eq. (1) is closely related to the value of  $p$ , namely,  $\text{Tr}(\rho_p^2) = (1 - \frac{2}{d})p^2 + \frac{p}{d} + \frac{1}{d}$ .

To achieve a unified notation for pure states and mixed states, a density matrix  $\rho$ , i.e., a  $d \times d$  matrix is utilized to describe a quantum state. Although there are many ways to generate a Hermitian operator, the condition of positivity is difficult to guarantee. Given any lower triangular matrix  $\rho_L$ , a physical density matrix can be obtained as

$$\rho = \frac{\rho_L \rho_L^\dagger}{\text{Tr}(\rho_L \rho_L^\dagger)}. \quad (2)$$

$\rho$  in Eq. (2) satisfies the three conditions of Hermitian, positive semidefinite and unit trace. In addition, according to the Cholesky decomposition [45], for any density matrix  $\rho$ , there exists a lower triangular matrix  $\rho_L$  that achieves  $\rho_L \rho_L^\dagger = \rho$ . Note that a tiny perturbation term (e.g.,  $\epsilon = 10^{-7}$ ) is usually added to the simulated pure states to avoid convergence issues using the Cholesky decomposition [45]

$$\rho = (1 - \epsilon)|\psi\rangle\langle\psi| + \frac{\epsilon}{d}\mathbb{I}_d. \quad (3)$$

Hence, the search for a physical quantum state can be converted to the search for a lower triangular matrix, which can be further transformed into a real vector by splitting the real and imaginary parts.

### 2.2. Quantum measurement settings

Theoretically, the minimum number of measurements to fully characterize a quantum state with dimension  $d$  is  $d^2$  [33]. For example, a linearly independent set of projectors

from pairwise combinations of eigenstates of the Pauli operators can be constructed [33]. An improved estimate of 2-qubit quantum states can be obtained when tomography is performed using projections onto 36 tensor products of Pauli eigenstates [46]. In addition, mutually unbiased bases where all inner products between projectors of different bases are equal to  $\frac{1}{d}$  have the potential to maximize information extraction per measurement [47]. Hence, the measurement operators play an important role in the estimation problem.

In this work, we consider two types of measurement settings: (i) tensor products of Pauli matrices, which is also called the cube measurement [46], (ii) the mutually unbiased bases (MUB) measurement [47]. For  $n$ -qubits, there are  $6^n$  measurement basis operators involved in cube measurement and  $(4^n + 2^n)$  involved in MUB measurement. Measurement basis states for cube and MUB are usually grouped into sets, with each set containing  $d = 2^n$  orthogonal projectors. Typically, the  $6^n$  measurement operators in cube are arranged into  $3^n$  sets. Similarly, the MUB measurements are grouped into  $(2^n + 1)$  sets. Detailed information is given in Appendix Appendix A.

In real applications, measurements usually suffer from noise. In this work, we consider unitary rotations on the measurement operators to simulate the noise. For 1-qubit, an arbitrary rotation operator can be defined as [48]

$$U(\theta_1, \theta_2, \theta_3) = \begin{bmatrix} e^{i\theta_1} \cos(\theta_2) & -ie^{i\theta_3} \sin(\theta_2) \\ -ie^{-i\theta_3} \sin(\theta_2) & e^{-i\theta_1} \cos(\theta_2) \end{bmatrix}. \quad (4)$$

For  $n$ -qubit systems, we consider the local noise, with the unitary rotation transformation defined as

$$U_e = U_{\Theta_1} \otimes U_{\Theta_2} \cdots \otimes U_{\Theta_n}, \quad (5)$$

where  $\Theta_k = (\theta_1^k, \theta_2^k, \theta_3^k)^T$  denotes the noise vector for the  $k$ -th qubit. The existence of unitary rotation noise in measurements makes the measurement projector change from  $M$  to  $U_e M U_e^\dagger$ .

### 2.3. DNN-QST

Quantum state tomography involves reconstructing quantum states based on measured statistics, e.g., observed frequencies. According to the universal approximation theorem [13], any continuous function on a compact subset of  $\mathbb{R}^n$  can be theoretically approximated by deep neural networks with multiple layers of fully connected neural networks. Hence, a multi-layer neural networks can be constructed to approximate a function mapping from measured frequencies to physical density matrices. Finally, QST is transformed into a regression problem, which can be solved in a supervised learning procedure.

For this regression problem, the input can be the observed frequencies, which depend on the choice of measurement operators. Recall the measurements are usually grouped into different sets, the dimension of the input vector is determined by the number of sets among the measurements. Hence, the input feature can be calculated

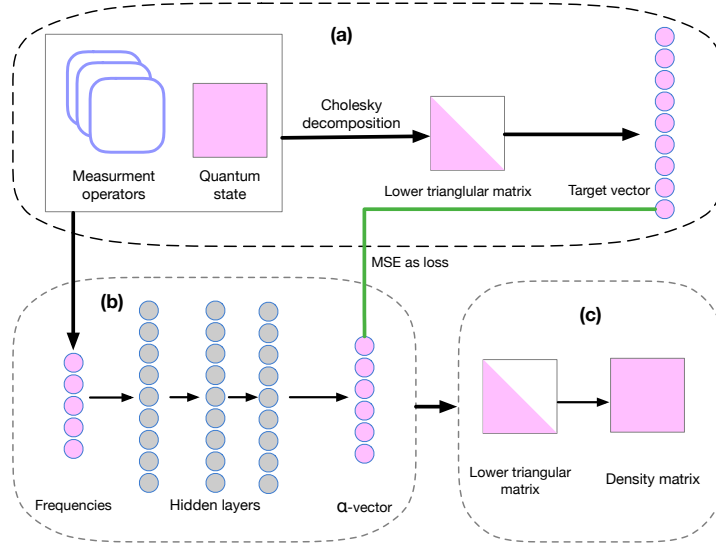


**Figure 1.** Schematic of the DNN-QST approach. (a) Obtain the measured data and compute the Cholesky decomposition of the density matrices as the target vectors; (b) A multi-layer neural network maps the frequencies to the  $\alpha$ -vector; (c) Obtain the quantum states from the networks' output.

as  $2^n K$ , with  $K$  the number of measurement sets. For example, for the complete measurement case, its input would be  $6^n$ -dimensional feature vectors for the cube measurement and  $2^n(2^n + 1)$ -dimensional feature vectors for the MUB measurement, respectively. While, for the incomplete case, the input dimension would decay.

Recall a lower triangular matrix  $\rho_L$  is correlated with a positive Hermitian matrix  $\rho$  in Eq. (2). When designing deep neural networks to reconstruct a quantum state, a lower triangular matrix  $\rho_L$  can be used as an intermediate state.  $\rho_L$  is a complex matrix with real and positive diagonal entries and complex off-diagonal elements, and thus can be further represented as a real vector with length  $d^2$  (defined as the  $\alpha$ -vector in this work). In particular, the positive diagonal entries are first ordered, and then the real and imaginary parts of off-diagonal elements are considered. As such, the output layer can be designed with  $d^2$  neurons to represent the  $\alpha$ -vector, which can be utilized to produce physical density matrices with additional transformations.

The schematic of DNN-QST is summarized in Figure 1. In (a), samples are generated from density matrices and measurement operators, and the useful data includes the measured frequencies and the target vectors calculated by the Cholesky decomposition. In (b), an architecture that includes input-hidden-output layers is utilized as a parameterized function to map a feature vector comprising of the measurement outcomes to the  $\alpha$ -vector, which is then transformed into a physical density matrix (see (c)). The loss function for training the neural networks adopts the mean squared error (MSE) between the reconstructed  $\alpha$ -vector (from the output of the neural networks) and the expected target vector (from the decomposition of the density matrix). Then, the networks are trained using a gradient descent algorithm with AdamOptimizer to minimize the MSE [49].

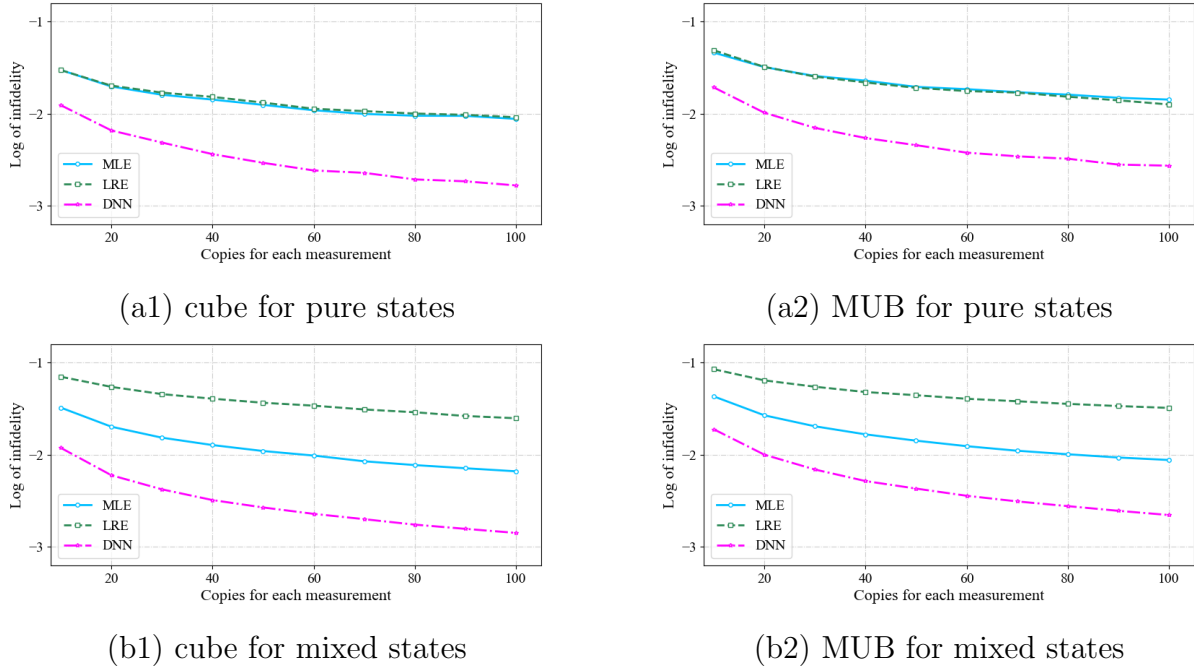


**Figure 2.** The performance of 2-qubit states for pure states and mixed states using few measurement copies. (a1) Infidelity vs copies for cube basis for pure states; (a2) Infidelity vs copies for MUB for pure states; (b1) Infidelity vs copies for cube basis for mixed states with  $p = 0.9$ ; (b2) Infidelity vs copies for MUB for mixed states with  $p = 0.9$ .

Reconstructing quantum states using DNN-QST is carried in two stages. In the first stage, the networks are iteratively optimized using the training samples and the parameters are updated with the purpose of minimizing the MSE. After the weights of the neural networks have been learnt, we come to the second stage, i.e., to apply the neural networks to reconstruct the density matrices of quantum states from new measurement outcomes. Unlike the training process, a procedure of  $\alpha \rightarrow \rho_L \rightarrow \rho$  is required to obtain physically valid quantum states. Although the first stage requires many iterations to optimize, the second stage only requires a single feed-forward calculation without iterations. From this perspective, DNN-QST is efficient in reconstructing quantum states.

### 3. Numerical results on QST with limited resources

In this section, parameter settings are first introduced, and then QST using few measurement copies and incomplete measurements is investigated and analyzed to demonstrate the effectiveness of DNN-QST compared with LRE and MLE.

### *3.1. Parameter settings*

For each case, a large number of samples are generated by randomly sampling the parameters. 98800 samples are used for training the parameters of DNN-QST. Then the DNN-QST model is tested on other 1000 samples. In addition, those 1000 samples are also tested on LRE and MLE. Detailed information about quantum measurement settings for cube and MUB are provided in Appendix Appendix A. For simulations, the Pytorch framework is utilized to construct the deep neural networks to run the model. In particular, three hidden layers are utilized, with each hidden layer using the same neurons. The number of neurons for the hidden layers is set as 128 for 2-qubit pure states, and is set as 256 for 2-qubit mixed states and 3-qubit states. All neurons are activated by the leaky relu function except the one before the  $\alpha$ -vector. For MLE, the iteration process is terminated once the gap of infidelity between two successive runs falls below  $10^{-8}$ . For LRE, a fast version of projection is performed to project a Hermitian operator with negative eigenvalues to a physical density operator [40]. To demonstrate the efficiency of the DNN-QST method, the infidelity of two states is defined as  $\bar{F} = 1 - F(\rho, \sigma)$ , with the fidelity between the reconstructed state and the real state defined as  $F(\rho, \sigma) = |\text{Tr}(\sqrt{\sqrt{\rho}\sigma\sqrt{\rho}})|$ .

### *3.2. Few copies*

In real applications, a measurement on quantum systems may return a statistical value of probability, i.e., frequency. Consider that an individual outcome only provides limited information on the estimated state, an infinite number of measurements is required to determine a quantum state precisely. However, only finite measurements are available in practical QST. In that case, the accuracy of measured frequencies can be influenced by the number of measurement copies used. In this subsection, we focus on the case of QST when the measurement copies are limited. In particular, we assume that the copies for each measurement are equal, denoted as  $S$ , and the total number of copies is  $N = Sk$  with  $k$  being the number of measurement operators.

Figure 2 demonstrates that the infidelity of the three methods decreases with the number of copies for each measurement on both the cube and the MUB measurement settings. For both pure states and mixed states with  $p = 0.9$  (purity  $\text{Tr}(\rho^2) = 0.88$ ), the performance of DNN is better than the other two methods, and the advantage of DNN over LRE and MLE becomes obvious with an increasing number of copies. Unlike the case of pure states where MLE and LRE achieve similar performance in Figure 2 (a1)-(a2), the two methods achieve different estimation fidelities when reconstructing mixed states in Figure 2 (b1)-(b2). The simulation of 2-qubit states with different purities has been implemented, with results provided in Appendix B. The results for 3-qubit pure states are summarized in Appendix C.



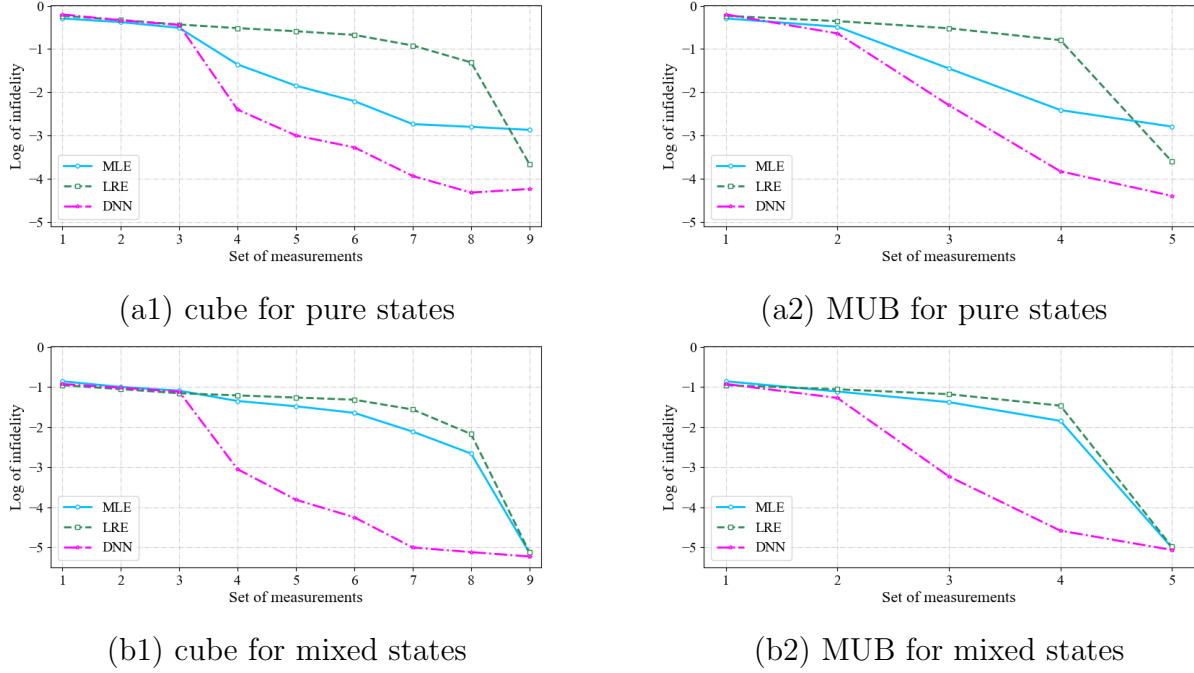
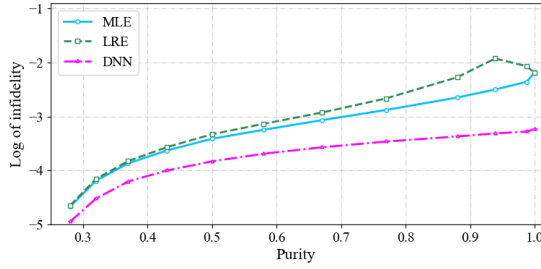


**Figure 3.** The performance of 2-qubit pure states and mixed states using incomplete measurements. (a1) Infidelity vs sets of the cube measurement for pure states; (a2) Infidelity vs sets of the MUB measurement for pure states; (b1) Infidelity vs sets of the cube measurement for mixed states with  $p = 0.5$ ; (b2) Infidelity vs sets of the MUB measurement for mixed states with  $p = 0.5$ .

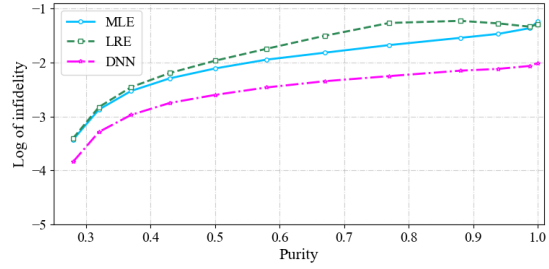
### 3.3. Incomplete measurements

For 2-qubit systems, we consider 9 cases for the cube setting, including cube1, cube2, ..., cube9 and 5 cases for the MUB setting, including mub1, mub2, ..., mub5. Note that cuben (mubn) includes the first  $n$  sets of projectors from the complete cube (MUB) measurement operators following the order in Tabel A1 (see in Appendix A). Since the measurement projectors are usually arranged into several sets, the incompleteness of measurement operators is defined with respect of the number of measurement sets.

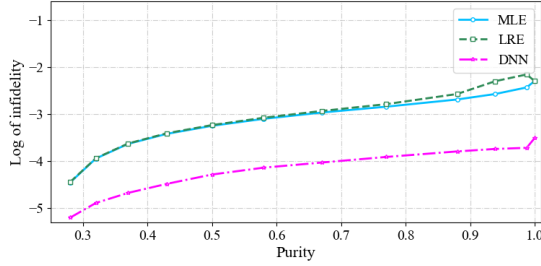
In Figure 3, DNN achieves better estimation accuracy than the other two methods for both pure states and mixed states with  $p = 0.5$  (purity  $\text{Tr}(\rho^2) = 0.5$ ). Also, LRE is sensitive to the completeness of measurement operators, since it achieves the worst performance when the number of sets is 4-8 for the cube measurement and 2-4 for the MUB measurement, but can achieve excellent infidelity for the complete cube and MUB measurements. Additionally, the simulation of 2-qubit states with different purities has been implemented, with results provided in Appendix B. The results for 3-qubit pure states are summarized in Appendix C.



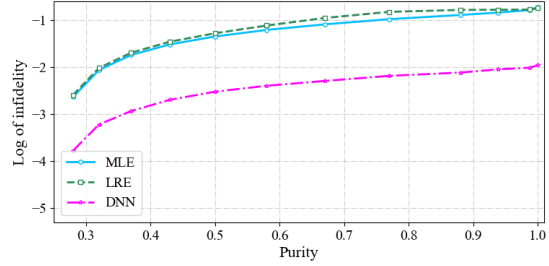
(a1) Gaussian noise with ratio 0.01



(a2) Gaussian noise with ratio 0.05

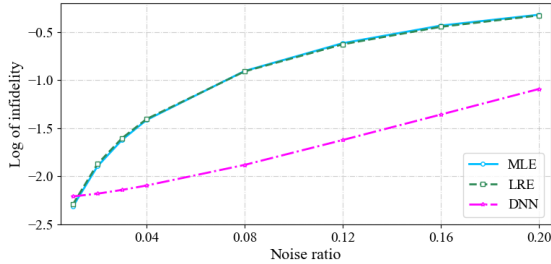


(b1) uniform noise with ratio 0.01

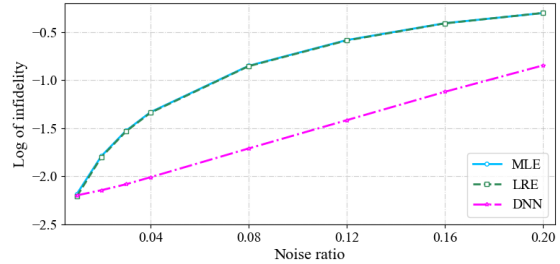


(b2) uniform noise with ratio 0.1

**Figure 4.** The performance of 2-qubit states with different purities using noisy cube measurement. (a1) Infidelity vs purity for Gaussian noise with ratio 0.01; (a2) Infidelity vs purity for Gaussian noise with ratio 0.05; (b1) Infidelity vs purity for uniform noise with ratio 0.01; (b2) Infidelity vs purity for uniform noise with ratio 0.1.



(a) cube



(b) MUB

**Figure 5.** The results of 2-qubit quantum states from the quantum optical device when measurement operators suffer from uniform noise. (a) Infidelity vs the noise ratio for the cube measurement; (b) Infidelity vs the noise ratio for the MUB measurement.

#### 4. Results on QST with noise

In this section, QST with noise is investigated. We use the same parameter settings in Section 3.1. Firstly, the performance of QST using measurement operators subject to different noises is compared and analyzed on 2-qubit and 3-qubit systems. Recall DNN-QST is typically trained using some training data, and can be tested for additional data with one step of feed-forward calculation without iteration. It is natural to ask whether the trained model can be directly evaluated on new data that follows a different distribution from the training data. Hence, we investigate the performance of DNN-QST

on quantum states coming from a quantum optical device without specific adjustment of the trained model.

#### 4.1. Numerical results for 2-qubit states

In this subsection, we focus on the case of measurement projectors suffering from unitary noise as in Eq. (5). In particular, we consider two types of unitary noise: (i) noise parameters follow Gaussian distributions (denoted as  $\mathcal{N}$ ); (ii) noise parameters follow uniform distributions (denoted as  $\mathcal{U}$ ). For simplicity, three ratios  $\xi_1, \xi_2$ , and  $\xi_3$  are introduced. The noise parameters for the first case are sampled as  $\theta_1 \sim \mathcal{N}(0, \pi\xi_1)$ ,  $\theta_2 \sim \mathcal{N}(0, 2\pi\xi_2)$ , and  $\theta_3 \sim \mathcal{N}(0, 2\pi\xi_3)$ . For the uniform cases, the noise parameters are sampled as  $\theta_1 \sim \mathcal{U}(0, 2\pi\xi_1)$ ,  $\theta_2 \sim \mathcal{U}(0, 0.5\pi\xi_2)$ , and  $\theta_3 \sim \mathcal{U}(0, 2\pi\xi_3)$ . In these cases, during the data collecting process, the measured frequencies are observed using the noisy operator  $U_e M U_e^\dagger$  rather than the ideal operator  $M$ . However, during the data analysis, the reconstruction algorithm utilizes the measurement projector  $M$ , since the noise parameters are not available during the simulations.

Figure 4 summarizes the results of 2-qubit states under different purities using the cube measurement. When measurement operators are subject to Gaussian or uniform noise, DNN ranks first, followed by MLE. The gap between LRE and MLE is wider for Gaussian noise than that for uniform noise. The infidelity of DNN and MLE increases with purity, while the infidelity of LRE first increases slowly and then drops greatly with purity. The results of estimating 3-qubit pure states using noisy cube measurements are provided in Appendix C. Additionally, the performance of estimating 2-qubit states with noisy MUB measurements is summarized in Appendix D.

#### 4.2. Results for quantum optical states

In this subsection, QST for quantum optical states is investigated. Since any binary quantum alternative of a photon can serve as a qubit, the polarization and path degrees of freedom can serve as two qubits. We follow the scheme in [21] to generate 2-qubit quantum states, with the schematic of experimental setup given in Appendix E. Under that scheme, 2-qubit unitary gates can be realized by combining a path unitary gate with a polarization gate [50]. Denote a 2-qubit unitary gate as  $U = \begin{bmatrix} U_{RR} & U_{RL} \\ U_{LR} & U_{LL} \end{bmatrix}$ , where

$U_{RR}, U_{RL}, U_{LR}$  and  $U_{LL}$  are  $2 \times 2$  matrices following the form of  $U_{RR} = \frac{1}{2}V_2(V_R + V_L)V_1$ ,  $U_{LL} = \frac{1}{2}(V_R + V_L)$ ,  $U_{RL} = -\frac{i}{2}V_2(V_R - V_L)$ , and  $U_{LR} = \frac{i}{2}(V_R - V_L)V_1$ . Thus, a set of quarter-wave plates (QWPs), half-wave plates (HWPs), and phase shifters may generate the unitary operators  $V_1, V_2, V_R$  and  $V_L$ . By performing 2-qubit unitary gate on the initial states, the output states are used for tomography.

We focus on mixed states with purity large than 0.99 and experimentally prepare five of them (also called as basis states) using the above optical device. To include more quantum optical states for testing, 1000 unitary gates are simulated on each basis state by sampling the parameters that are associated with  $V_1, V_2, V_R$  and  $V_L$ . Finally,

5005 quantum optical states are obtained for the following comparison. To test the generalization of DNN-QST, we directly adopt the model trained using the quantum states sampled according to Eq. (1) with  $p = 0.99$  in the above subsection, and test it on 5005 quantum optical states. The observed statistics for measuring the testing states are numerically simulated. The results of reconstructing those quantum optical states using noisy measurements are revealed in Figure 5. As is shown, LRE and MLE achieve similar performance and DNN achieves better performance with increasing noise ratios for both the cube and the MUB measurements. Based on these results, DNN-QST has strong generalization in estimating quantum optical states and exhibits robustness against errors in the measurement operators.

## 5. Conclusion

Quantum state tomography is a significant task that has implications for many other quantum information processing tasks. Owing to the potential of ML to capture complex patterns from data, we proposed a general framework that utilizes neural networks to estimate quantum states with constrained measurements. To demonstrate its efficiency, we applied it to three cases, including few measurement copies and incomplete measurements as well as noisy measurement operators. Numerical results demonstrate that DNN-QST has a great potential to achieve higher efficiency than LRE and MLE when estimating states with limited resources. Besides, DNN-QST is efficient in dealing with the noise in measurement operators and exhibits favorable robustness when reconstructing quantum optical states with noisy measurements. Our future work will focus on adaptative QST using ML and taking the advantages of ML to speed up tomography-based quantum experiments.

## Acknowledgments

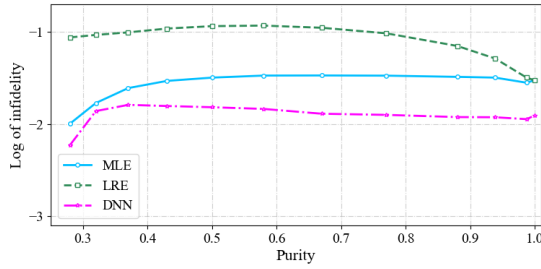
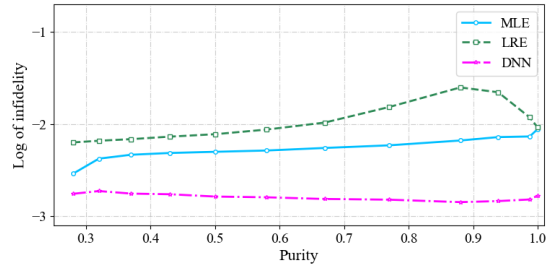
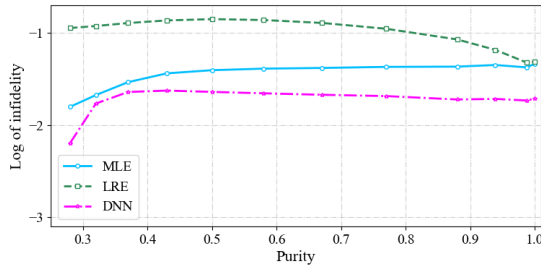
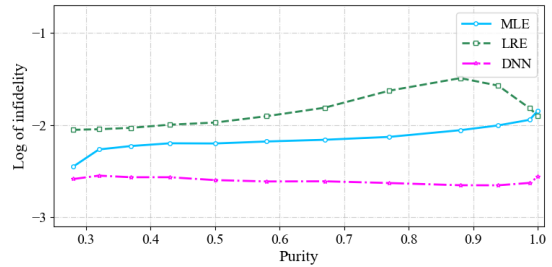
This work was supported by the Australian Research Council’s Future Fellowship funding scheme under Project FT220100656, and the Australian Research Council’s Discovery Projects funding scheme DP210101938, and U.S. Office of Naval Research Global under Grant N62909-19-1-2129.

## Appendix A. Detailed information about quantum measurements

Let the eigen-vectors of  $\sigma_x$  be the diagonal state  $|D\rangle$  and the anti-diagonal state  $|A\rangle$ . Define the eigen-vectors of  $\sigma_y$  as the left circular polarization state  $|L\rangle$  and the right circular polarization state  $|R\rangle$  and take the eigen-vectors of  $\sigma_z$  as the horizontal state  $|H\rangle$  and the vertical state  $|V\rangle$ . These six basis states form the 1-qubit Pauli measurement [46],  $P_{\text{pauli}} = \{|H\rangle, |V\rangle, |D\rangle, |A\rangle, |R\rangle, |L\rangle\}$ . They are informationally complete for reconstructing 1-qubit quantum states. For 2-qubit case, their measurement basis states are summarized in Table A1.

**Table A1.** The measurement bases used in cube and MUB.

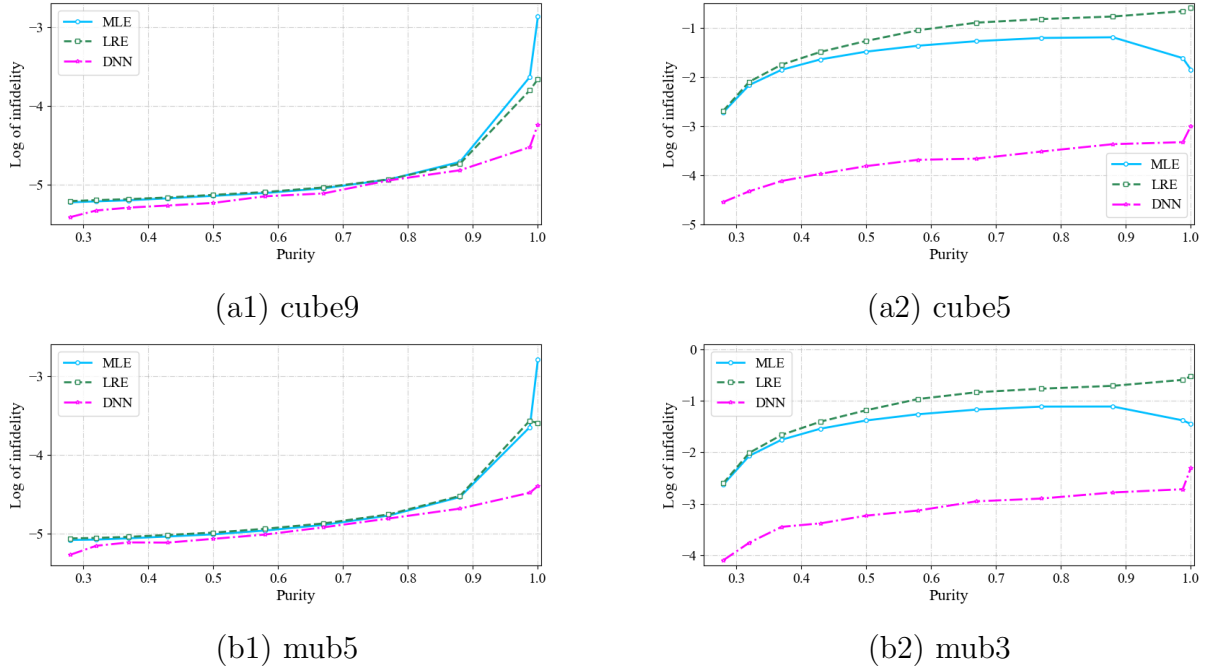
cube	MUB
$ HH\rangle,  HV\rangle,  VH\rangle,  VV\rangle$	$ HH\rangle,  HV\rangle,  VH\rangle,  VV\rangle$
$ HD\rangle,  HA\rangle,  VD\rangle,  VA\rangle$	$ RD\rangle,  RA\rangle,  LD\rangle,  LA\rangle$
$ HR\rangle,  HL\rangle,  VR\rangle,  VL\rangle$	$ DR\rangle,  DL\rangle,  AR\rangle,  AL\rangle$
$ DH\rangle,  DV\rangle,  AH\rangle,  AV\rangle$	$\frac{1}{\sqrt{2}}( RL\rangle + i LR\rangle), \frac{1}{\sqrt{2}}( RL\rangle - i LR\rangle),$
$ DD\rangle,  DA\rangle,  AD\rangle,  AA\rangle$	$\frac{1}{\sqrt{2}}( RR\rangle + i LL\rangle), \frac{1}{\sqrt{2}}( RR\rangle - i LL\rangle)$
$ DR\rangle,  DL\rangle,  AR\rangle,  AL\rangle$	$\frac{1}{\sqrt{2}}( RV\rangle + i LH\rangle), \frac{1}{\sqrt{2}}( RV\rangle - i LH\rangle),$
$ RH\rangle,  RV\rangle,  LH\rangle,  LV\rangle$	$\frac{1}{\sqrt{2}}( RH\rangle + i LV\rangle), \frac{1}{\sqrt{2}}( RH\rangle - i LV\rangle)$
$ RD\rangle,  RA\rangle,  LD\rangle,  LA\rangle$	
$ RR\rangle,  RL\rangle,  LR\rangle,  LL\rangle$	


 (a1) cube with  $S = 10$ 

 (a2) cube with  $S = 100$ 

 (b1) MUB with  $S = 10$ 

 (b2) MUB with  $S = 100$ 

**Figure B1.** The performance for 2-qubit states with different purities using few measurement copies. (a1) Infidelity vs purity for cube basis with  $S = 10$ ; (a2) Infidelity vs purity for cube basis with  $S = 100$ ; (b1) Infidelity vs purity for MUB with  $S = 10$ ; (b2) Infidelity vs purity for MUB with  $S = 100$ .

## Appendix B. Results for QST with limited resources on 2-qubit states

The results for estimating 2-qubit states with different purities using few copies are shown in Figure B1. For  $S = 10$  and  $S = 100$ , DNN achieves the best performance under both the cube measurement and the MUB measurement, followed by MLE. Also, graphs of infidelity vs purity for the three methods exhibit different trends. In particular, the infidelity of MLE increases with purity, while the infidelity of LRE first increases slowly and then drops greatly with purity. By comparison, the infidelity of DNN first



**Figure B2.** The performance of 2-qubit states with different purities using incomplete measurements. (a1) Infidelity vs purity for cube9; (a2) Infidelity vs purity for cube5; (b1) Infidelity vs purity for mub5; (b2) Infidelity vs purity for mub3.

increases until around purity of 0.35 and drops slowly with purity for  $S = 10$ , and the infidelity of DNN nearly keeps the same with tiny fluctuation for  $S = 100$ .

The results of estimating 2-qubit states with different purities using incomplete measurements are shown in Figure B2. DNN achieves the best fidelity for both the cube and the MUB measurements. Besides, LRE is superior to MLE for the complete measurements in (a1) and (b1), but is worse than MLE for incomplete measurements including cube5 and mub3. Besides, the curves of infidelity versus purity for the three methods exhibit different trends. In particular, the infidelity of DNN always increases with purity for the four cases, which is similar to that of LRE. By comparison, the infidelity of MLE increases with purity for complete measurements, but exhibits a trend of first increasing and then dropping with purity for incomplete measurements.

### Appendix C. Numerical results for 3-qubits

In this section, we provide numerical results of 3-qubit pure states following the Haar metric. Figure C1 summarizes the results for QST with few copies, where the estimation accuracy of the three methods improves with increasing number of copies for each measurement. In particular, DNN achieves the lowest infidelity, while MLE is better than LRE with an increasing number of measurement copies. The numerical results demonstrate that the proposed method has the potential to achieve efficient QST for both pure and mixed states using a limited number of copies.

In addition, the simulation results of QST using incomplete measurements are

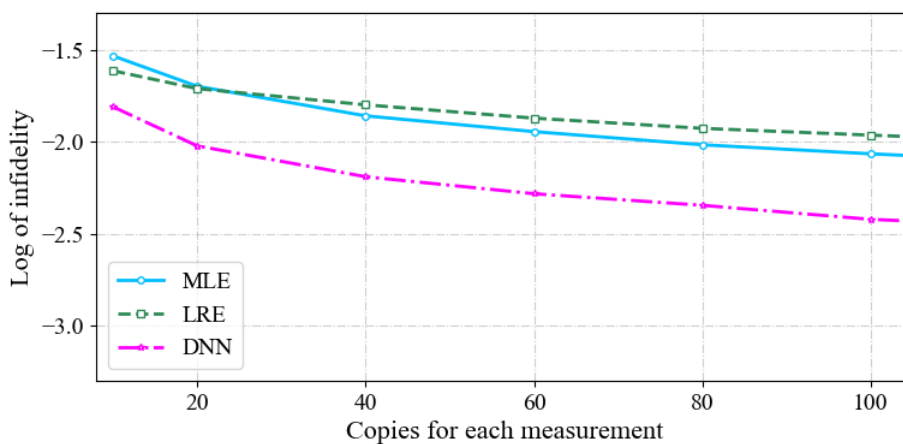


**Figure C1.** Results for 3-qubit random pure states when the cube measurement has few copies.

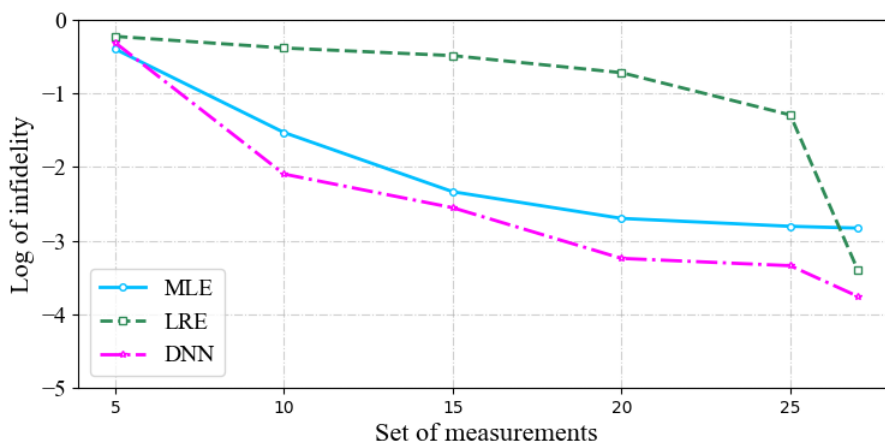


**Figure C2.** Results for 3-qubit random pure states using different numbers of measurement sets for the cube measurement.

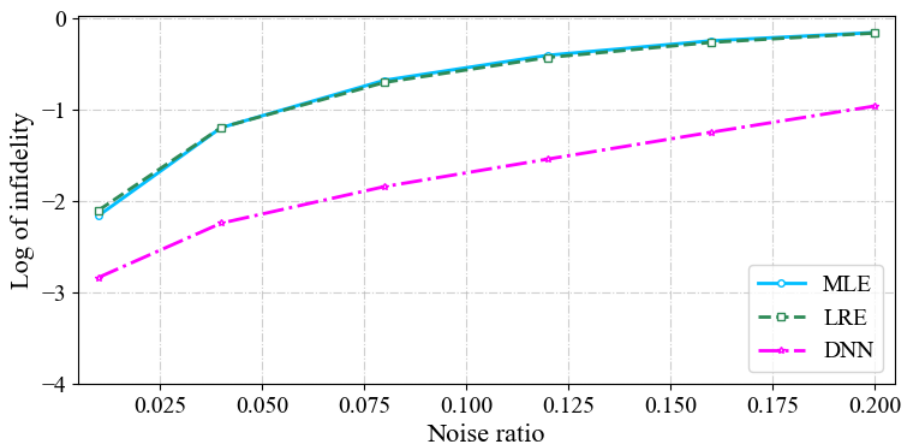
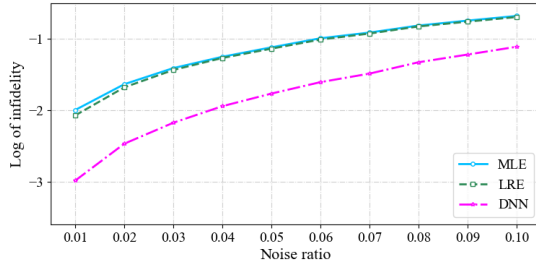
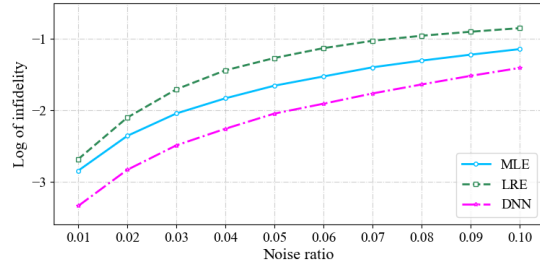


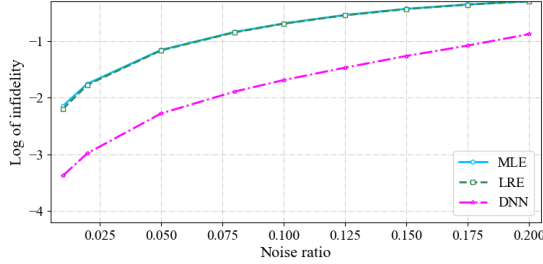
**Figure C3.** Results for 3-qubit random pure states when the cube measurement suffers from uniform noise.



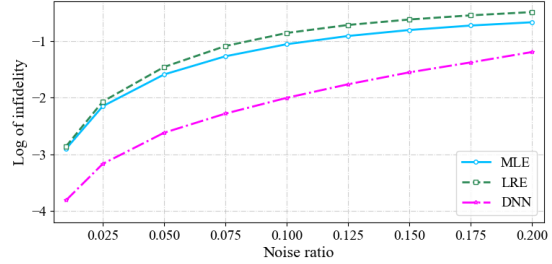
(a1) Gaussian noise for pure states



(a2) Gaussian noise for mixed states



(b1) uniform noise for pure states



(b2) uniform noise for mixed states

**Figure D1.** The performance of 2-qubit pure states and mixed states using noisy MUB measurement. (a1) Infidelity vs noise ratio (Gaussian noise) for pure states; (a2) Infidelity vs noise ratio (Gaussian noise) for mixed states with  $p = 0.7$ ; (b1) Infidelity vs noise ratio (uniform noise) for pure states; (b2) Infidelity vs noise ratio (uniform noise) for mixed states with  $p = 0.7$ .

summarized in Figure C2, where LRE fails to achieve good infidelity when the measurement set is close to the complete case, suggesting that LRE is sensitive to the completeness of measurements. By comparison, DNN achieves better estimation than MLE with few measurement operators. Based on the above results, DNN has the advantage of reconstructing quantum states using incomplete measurements.

The results of QST with noise are summarized in Figure C3, where LRE and MLE achieve similar performance when the cube measurement suffers from uniform noise. Compared with the two methods, DNN exhibits a superior performance under different noise ratios. The above results verify that DNN-QST is powerful in estimating 3-qubit pure states in both limited resources and noisy measurements.

#### Appendix D. Results of QST with noise on 2-qubit states

The numerical results of 2-qubit states when the MUB measurement suffers from different noise ratios is summarized in Figure D1. The performance of DNN is better than the other two methods, although its infidelity increases with increasing noise ratios. Also, MLE and LRE achieve similar performance for pure states but exhibit different results for mixed states, especially for Gaussian noise.



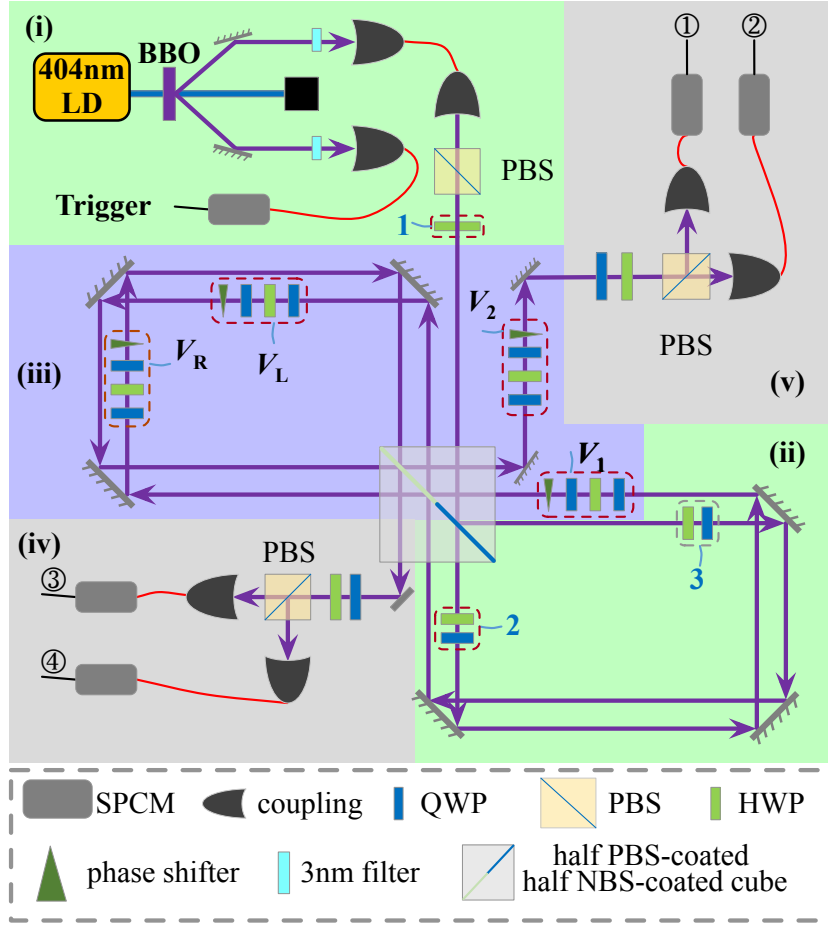


**Figure E1.** The schematic of experimental setup for 2-qubit quantum optical device. The setup includes into three modules. (i)-(ii) State preparation, (iii) Unitary gate, (iv)-(v) Measurements.

## Appendix E. Detailed information about quantum optical device

We follow the scheme in [21] to generate 2-qubit quantum states on quantum optical device. As in Figure E1, the experimental setup is divided into three modules. 1) **State preparation** (Figure E1. (i)-(ii)): Phase-stable 2-qubit states are generated from a Sagnac interferometer. Photon pairs are produced using type-I spontaneous parametric down-conversion (SPDC) in a nonlinear crystal (BBO), with one prepared in the state of  $|H\rangle$  via a polarized beam splitter (PBS) and the other sent to a single photon counting module (SPCM) as a trigger. Then a half-wave plate (HWP) along with a PBS controls the path qubit of the photon. The polarization of the photon in each path is manipulated by an HWP and a quarter-wave plate (QWP). 2) **Unitary gate** (Figure E1. (iii)): 2-qubit unitary gate is produced from another interferometer. A special beam splitter cube that is half PBS coated and half coated by a non-polarizer beam splitter (NBS) is applied in the junction of two Sagnac interferometers. Then four unitary polarization operators  $V_1$ ,  $V_2$ ,  $V_R$  and  $V_L$  are generated from the combination of two QWPs, an HWP, and a phase shifter (PS) composed of a pair of wedge-shaped

plates. 3) **Measurements** (Figure E1. (iv)-(v)): Measurements can be realized with the combination of a QWP, an HWP and a PBS.

## References

- [1] Wiseman H M and Milburn G J 2009 *Quantum Measurement and Control* (Cambridge University Press)
- [2] Dong D and Petersen I R 2022 *Annual Reviews in Control* **54** 243–251
- [3] Nielsen M A and Chuang I L 2010 *Quantum Computation and Quantum Information* (Cambridge University Press)
- [4] Dong D and Petersen I R 2010 *IET Control Theory & Applications* **4** 2651–2671
- [5] Gisin N and Thew R 2007 *Nature Photonics* **1** 165–171
- [6] Opatrný T, Welsch D G and Vogel W 1997 *Physical Review A* **56** 1788
- [7] Huszár F and Houlby N M 2012 *Physical Review A* **85** 052120
- [8] Blume-Kohout R 2010 *New Journal of Physics* **12** 043034
- [9] Řeháček J, Hradil Z and Ježek M 2001 *Physical Review A* **63** 040303
- [10] Ježek M, Fiurášek J and Hradil Z 2003 *Physical Review A* **68** 012305
- [11] Qi B, Hou Z, Li L, Dong D, Xiang G and Guo G 2013 *Scientific Reports* **3** 3496
- [12] Qi B, Hou Z, Wang Y, Dong D, Zhong H S, Li L, Xiang G Y, Wiseman H M, Li C F and Guo G C 2017 *npj Quantum Information* **3** 19
- [13] LeCun Y, Bengio Y and Hinton G 2015 *Nature* **521** 436–444
- [14] Goodfellow I, Bengio Y and Courville A 2016 *Deep Learning* (MIT Press)
- [15] Biamonte J, Wittek P, Pancotti N, Rebentrost P, Wiebe N and Lloyd S 2017 *Nature* **549** 195
- [16] Carleo G and Troyer M 2017 *Science* **355** 602–606
- [17] Lennon D, Moon H, Camenzind L, Yu L, Zumbühl D, Briggs G, Osborne M, Laird E and Ares N 2019 *npj Quantum Information* **5** 79
- [18] Fösel T, Tighineanu P, Weiss T and Marquardt F 2018 *Physical Review X* **8** 031084
- [19] Dong D and Petersen I R 2023 *Learning and Robust Control in Quantum Technology* (Springer Nature, Switzerland AG)
- [20] Ma H, Dong D, Ding S X and Chen C 2022 *IEEE Transactions on Neural Networks and Learning Systems*
- [21] Huang C J, Ma H, Yin Q, Tang J F, Dong D, Chen C, Xiang G Y, Li C F and Guo G C 2020 *Physical Review A* **102** 032412
- [22] Ma H, Huang C J, Chen C, Dong D, Wang Y, Wu R B and Xiang G Y 2023 *Automatica* **147** 110659
- [23] Xu Q and Xu S 2018 *arXiv preprint arXiv:1811.06654*
- [24] Ma H, Dong D and Petersen I R 2021 On how neural networks enhance quantum state tomography with limited resources *60th IEEE Conference on Decision and Control (CDC)*, pp. 4146–4151
- [25] Lohani S, Kirby B, Brodsky M, Danaci O and Glasser R T 2020 *Machine Learning: Science and Technology* **1** 035007
- [26] Danaci O, Lohani S, Kirby B and Glasser R T 2021 *Machine Learning: Science and Technology* **2** 035014
- [27] Lohani S, Searles T A, Kirby B T and Glasser R T 2021 *IEEE Transactions on Quantum Engineering* **2** 2103410
- [28] Ahmed S, Muñoz C S, Nori F and Kockum A F 2021 *Physical Review Letters* **127** 140502
- [29] Ahmed S, Munoz C S, Nori F and Kockum A F 2021 *Physical Review Research* **3** 033278
- [30] Neugebauer M, Fischer L, Jäger A, Czischek S, Jochim S, Weidemüller M and Gärttner M 2020 *Physical Review A* **102** 042604
- [31] Palmieri A M, Kovlakov E, Bianchi F, Yudin D, Straupe S, Biamonte J D and Kulik S 2020 *npj Quantum Information* **6** 20

- [32] Hou Z, Zhong H S, Tian Y, Dong D, Qi B, Li L, Wang Y, Nori F, Xiang G Y, Li C F *et al.* 2016 *New Journal of Physics* **18** 083036
- [33] James D F V, Kwiat P G, Munro W J and White A G 2001 *Physical Review A* **64**(5) 052312
- [34] Liu Y x, Wei L and Nori F 2004 *EPL (Europhysics Letters)* **67** 874
- [35] Chantasri A, Pang S, Chalermputitarak T and Jordan A N 2019 *Quantum Studies: Mathematics and Foundations* 1–25
- [36] Gonçalves D, Lavor C, Gomes-Ruggiero M, Cesário A, Vianna R and Maciel T 2013 *Physical Review A* **87** 052140
- [37] Teo Y S, Stoklasa B, Englert B G, Řeháček J and Hradil Z 2012 *Physical Review A* **85** 042317
- [38] Zorzi M, Ticozzi F and Ferrante A 2013 *IEEE Transactions on Information Theory* **60** 357–367
- [39] Maciel T O, Cesário A T and Vianna R O 2011 *International Journal of Modern Physics C* **22** 1361–1372
- [40] Smolin J A, Gambetta J M and Smith G 2012 *Physical Review Letters* **108** 070502
- [41] Torlai G and Melko R G 2020 *Annual Review of Condensed Matter Physics* **11** 325–344
- [42] Koutný D, Motka L, Hradil Z, Řeháček J and Sánchez-Soto L L 2022 *Physical Review A* **106** 012409
- [43] Wang Y, Cheng S, Li L and Chen J 2022 *arXiv preprint arXiv:2207.05341*
- [44] Mezzadri F 2006 *arXiv preprint math-ph/0609050*
- [45] Higham N J 1990 *Analysis of the Cholesky Decomposition of a Semi-definite Matrix* (Oxford University Press)
- [46] De Burgh M D, Langford N K, Doherty A C and Gilchrist A 2008 *Physical Review A* **78** 052122
- [47] Adamson R and Steinberg A M 2010 *Physical Review Letters* **105** 030406
- [48] Zyczkowski K and Kus M 1994 *Journal of Physics A: Mathematical and General* **27** 4235
- [49] Kingma D P and Ba J 2015 Adam: A method for stochastic optimization *Proceedings of International Conference on Learning Representations*
- [50] Englert B G, Kurtsiefer C and Weinfurter H 2001 *Physical Review A* **63** 032303